

## Comparative Vibrational analysis, Electronic Properties, and molecular docking of Lantadene A and B (Potential anticancer agents) - A Computational DFT Study

Anoop Kumar Pandey<sup>1</sup>, Shashwat Shukla<sup>1</sup>, O.P. Yadav<sup>1</sup>, Vijay Singh<sup>2</sup>, Apoorva Dwivedi<sup>3\*</sup>

<sup>1</sup>Department of Physics, K. S. Saket P.G. College, Ayodhya, India.

<sup>2</sup>University of Dodoma, Dodoma, Tanzania.

<sup>3</sup>Department of Applied Science and Humanities, Seth Vishambhar Nath Institute of Engineering and Technology, Barabanki, India.

\*Corresponding author: Apoorva Dwivedi, email: [apoorvahri@gmail.com](mailto:apoorvahri@gmail.com); Phone: +919415289670.

Received May 2<sup>nd</sup>, 2023; Accepted January 22<sup>nd</sup>, 2024.

DOI: <http://dx.doi.org/10.29356/jmcs.v68i3.2060>

**Abstract.** We conducted a comprehensive analysis of Lantadene A and B using FTIR spectroscopy, beginning with geometry optimization. Subsequently, we calculated their fundamental vibrational frequencies and intensities using the B3LYP/6-311G (d, p) method. To provide a thorough vibrational assignment, we utilized potential energy distribution (PED). The results from our calculated spectra closely matched the experimental data, demonstrating the accuracy of our calculations. Furthermore, we assessed the electronic properties of Lantadene A and B. We computed the HOMO-LUMO gap and visualized the frontier orbital HOMO-LUMO surfaces, as well as Molecular Electrostatic Potential (MEP) surfaces. These analyses shed light on the reactive nature of these compounds, highlighting their potential applications. Moreover, our investigation explored the hyperpolarizability values, suggesting that Lantadene A and B hold promise for electro-optical applications due to their unique properties. Additionally, we conducted docking studies of Lantadene A and Lantadene B with BCL2L1 (BCL2 like 1) and IKBKB (inhibitor of nuclear factor kappa B kinase subunit beta) proteins, as provided by HGNC. These analyses revealed promising interactions, supporting the potential use of Lantadene A and B as agents with anti-cancer and anti-inflammatory properties. In summary, our research indicates that Lantadene A and B possess properties that make them strong candidates for use in the development of anticancer and anti-inflammatory agents, while also showing promise for electro-optical applications.

**Keywords:** Lantadene A and B; vibrational analysis; DFT; HOMO-LUMO and MESP; molecular docking.

**Resumen.** Utilizando la espectroscopía de FTIR realizamos un análisis integral de lantadeno A y B, empezando con la optimización de sus geometrías. Después, calculamos las frecuencias e intensidades de vibración utilizando el método B3LYP/6-311G (d, p). Para realizar una asignación vibracional exhaustiva, utilizamos la distribución de energía potencial (PED). Los espectros calculados están en buen acuerdo con los experimentales, lo cual demuestra la precisión de nuestros cálculos. Además, evaluamos las propiedades electrónicas de lantadeno A y B. Calculamos la brecha (gap) HOMO-LUMO, visualizamos las isosuperficies de los orbitales frontera, y también las isosuperficies del potencial electrostático molecular (MEP). Estos análisis ayudan a esclarecer la reactividad de estas moléculas, destacando sus aplicaciones potenciales. Se exploraron los valores de las hiperpolarizabilidades las cuales sugieren que el lantadeno A y B son compuestos prometedores para aplicaciones electroópticas. Adicionalmente, se realizaron estudios de acoplamiento molecular de lantadeno A y B con las proteínas BCL2L1 (BCL2 como 1) y IKBKB (inhibidor del factor kappa B de la subunidad beta quinasa), que se obtuvieron del HGNC. Estos análisis mostraron interacciones prometedoras, que apoyan el uso potencial de lantadeno A y B

como agentes anticancerígenos y con propiedades antiinflamatorias. En síntesis, nuestra investigación indica que las propiedades del lantadeno A y lantadeno B las hacen buenos candidatos para su uso en el desarrollo de agentes anticancerígenos y antiinflamatorios, además de también mostrar potencial en aplicaciones electroópticas.

**Palabras clave:** Lantadeno A y B; análisis vibracional; DFT; HOMO-LUMO y MESP; acoplamiento molecular.

---

## Introduction

Natural products have long captivated researchers for various reasons, including their potential as antibiotics and pharmacologically active agents. They offer immense promise for exploring the cellular processes they can inhibit. Fundamental and conformational studies help formulate hypotheses about their interactions with target ligands, while synthesis allows us to test these hypotheses by eventually creating derivatives [1,2]. Among these natural products, *Lantana camara*, a flowering decorative plant, has been used in traditional medicinal preparations to treat a range of ailments. It serves as a rich source of diverse classes of bioactive natural metabolites. Throughout history, its flowers, leaves, and fruits have been applied externally to treat wounds, cuts, and skin diseases. Additionally, the stems, leaves, and roots of *Lantana camara* were employed for gargles and to alleviate toothaches in ancient times [3-5]. Interestingly, toxin research from *Lantana* leaves has revealed two molecular forms, of which only one has been found to be hepatotoxic to guinea pigs [6]. Various pharmaceutical properties of the *Lantana* plant have been documented in the literature [7,8]. Extracts isolated from *Lantana* leaves have demonstrated antitumor activity [9], antithrombin activity [10], as well as anti-inflammatory, anti-nociceptive, and antipyretic effects [11]. In a study at the Central Drug Research Institute, the stem of *Lantana camara* exhibited anti-filarial activity [12]. Literature reports also indicate the presence of significant bioactive compounds in *L. camara*, such as lantadene A, lantadene B, lantadene C, and lantadene D, which have been isolated from its aerial parts [13-15]. Lantadenes, derived from this plant, have shown a wide range of pharmacological activities, including antitumor properties [16-17]. These compounds differ in the structure of the side chain attached at the C-22 position, suggesting that these structural variations play a crucial role in their pharmacological activities [18-21]. Notably, Lantadene A and Lantadene B are the primary triterpene components of the red variety of *Lantana Camara*.

In the realm of computational chemistry, Density Functional Theory (DFT) has emerged as the preferred electronic structure theory for both molecular and extended systems. Concurrently, docking methodology has become a standard computational tool in drug design, aiding in predicting the binding modes and affinities of small molecules within specific receptor targets. This approach is instrumental in lead compound optimization and virtual screening studies to discover novel biologically active molecules.

Given the significance of these theories [22-26], we have undertaken a comprehensive investigation involving Comparative Molecular Docking, Experimental FT-IR Spectra, UV-Vis Spectra, Vibrational Analysis, Electronic Properties, and Fukui Function Analysis of Lantadene A and B compounds with medicinal potential.

## Experimental details and computational methods

The FTIR spectrum of the investigated compound has been recorded in Perkin-Elmer spectrometer in the range of 4000–500 $\text{cm}^{-1}$ . The frequencies of all sharp bands are accurate to  $\pm 1 \text{ cm}^{-1}$ . The molecular structures of the title compounds A and B are made by molecular modeling. The model molecular structures of the compounds are given in Figures 1 and 2. Initial geometry was generated from the standard geometrical parameters and was minimized without any constraint in the potential energy surface. The gradient corrected Density Functional Theory (DFT) with the three-parameter hybrid functional (B3) [27] for the exchange part and the Lee-Yang-Parr (LYP) correlation function [28] has been employed for the computation of molecular structure, vibrational frequencies, HOMO-LUMO, and energies of the optimized structures, using GAUSSIAN 09 [29]. The calculated vibrational frequencies have also been scaled by a factor of 0.963 [30]. By combining the results of the GAUSSVIEW'S program [31] with symmetry considerations, vibrational frequency

assignments were made with a high degree of accuracy. The prediction of IR frequencies of title compound has been found to be very straightforward using this approach. To determine the form of the modes we used the potential energy distribution (PED) calculations and applied the VEDA program performing both the PED analysis and its optimization [32]. Density functional theory calculations are reported to provide excellent vibrational frequencies of organic compound if the calculated frequencies are scaled to compensate for the approximate treatment of electron correlation, for basis set deficiencies and for anharmonicity. A number of studies have been carried out regarding calculations of vibrational spectra by using B3LYP methods with 6-311 G (d, p) basis set. The scaling factor (0.963) was applied successfully for B3LYP method and was found to be easily transferable in a number of molecules. Thus, vibrational frequencies calculated by using the B3LYP functional with 6-311G (d, p) as basis set, can be utilized to eliminate the uncertainties in the fundamental assignment in the IR spectra. The docking action of Lant A and Lant B with selected protein has been performed by Auto Dock 4.2 software. The molecular docking indicates binding action of drug with appropriate protein.

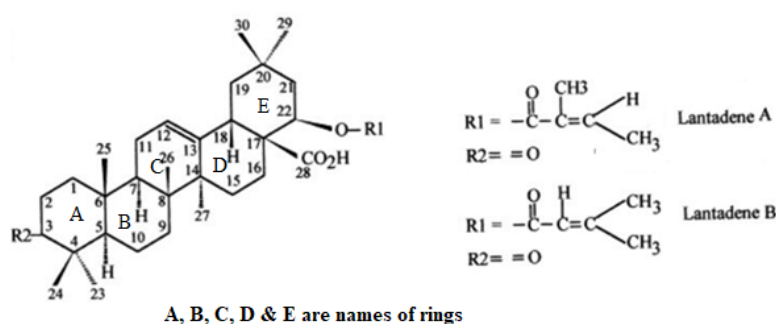


Fig. 1. Structures of Different Lantadene compounds.

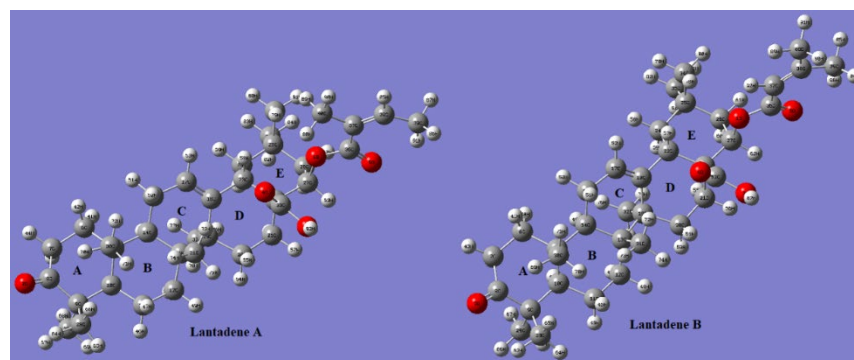


Fig. 2. Model Molecular Structure of Lantadene A and B.

## Results and discussion

The accuracy of Density Functional Theory (DFT) results, particularly when using the B3LYP functional and the 6-311 G (d, p) basis set, depends on several factors, including the specific system or molecule under investigation, the level of theory used, and the properties of interest. B3LYP is a widely used hybrid functional that combines the Becke88 exchange functional with the Lee-Yang-Parr (LYP) correlation functional. The 6-311G (d, p) basis set is a commonly used basis set that includes polarization functions (d functions) on non-hydrogen atoms and diffuse functions (p functions) on hydrogen atoms. It is a good general-purpose basis set. Accurate geometry optimization is crucial for obtaining reliable results. Ensure that the

optimization converges to a true minimum on the potential energy surface. Use tight convergence criteria and consider potential energy surface scans to explore different conformations.

### Geometry optimization

The geometry optimization of Lant A and B is obtained by B3LYP/6-311 G (d, p) method. The energy of optimized Lant A and B at ground state is -1740.6908 a.u. and -1741.474 a.u. respectively. The optimized geometries of Lant A and B in plane drawing and 2 D dimensions are presented in Figures 1 and 2 respectively. The A/B and B/C rings are in trans conformation while the D/E rings are cis fused. The packing of the molecule is stabilized by O--H...O hydrogen bonds. Bond lengths and angles (supplementary Table 1) agree with the values observed in similar compounds as maytenfolic acid.

**Table 1.** Calculated electronic transitions: E (eV), oscillatory strength (f),  $\lambda_{\max}$ (nm) using TD-DFT/B3LYP/6-311G(d,p) method.

S. No.	Electronic Transition	E (eV)	Osci.Str. (f)	Cal. ( $\lambda_{\max}$ )	% Contribution	Assignment
<b>Lantadene A</b>						
1	HOMO-1→ LUMO+1 HOMO→LUMO+1	4.26	0.0003	291	95 2	$n_p \rightarrow R_y^*$
2	HOMO→LUMO HOMO -4→LUMO	4.71	0.0002	263	93 5	$n_p \rightarrow R_y^*$
3	HOMO -4→LUMO HOMO 3→LUMO HOMO→LUMO	4.81	0.0005	258	80 12 5	$n_p \rightarrow R_y^*$
<b>Lantadene B</b>						
1	HOMO-1→LUMO+1	4.26	0.0003	291	95	$n_p \rightarrow R_y^*$
2	HOMO→LUMO	4.59	0.0002	270	98	$n_p \rightarrow R_y^*$
3	HOMO-4→LUMO HOMO-3→LUMO	4.79	0.0003	259	92 4	$n_p \rightarrow R_y^*$

### PES scan of lant A and lant B

We conducted a Potential Energy Surface (PES) scan to explore the dihedral angles C22-C33-O3-H92 and C22-C33-O3-H87, with values of 177.710 and 177.770, respectively, in both Lantadene A and Lantadene B. This scan involved a total of 36 steps, with 10 steps for each angle in both compounds. We employed the HF/6-31G level of theory for these initial scans. The resulting data was used to generate Relative Energy vs. Scan Coordinate plots for Lantadene A and Lantadene B, as shown in Supplementary Fig. S1 and S2. The minimum energy configurations were identified at dihedral angles C22-C33-O3-H92=177.71 and C22-C33-O3-H87=177.77 for both Lantadene A and Lantadene B, after performing the PES scan.

To refine our understanding of these minima, we subjected the initial geometries corresponding to these energy minima in Lantadene A and Lantadene B to further optimization. For this optimization, we utilized a combination of the DFT/B3LYP method and the 6-311G (d,p) basis set, which is known for its accuracy in describing molecular structures and properties.

In summary, our study involved a thorough investigation of the potential energy surfaces of Lantadene A and Lantadene B, focusing on specific dihedral angles of interest. The resulting data and optimized geometries will contribute to a better understanding of the structural properties and behaviors of these compounds.

### Vibrational analysis

Assignments of the FTIR (supplementary Fig. 3) frequencies are achieved by comparing the band positions and intensities observed in the FTIR spectra with wave numbers and intensities from molecular modeling calculations. The molecules Lantadene A and B both have 92 atoms with 270 normal modes of vibration. The calculated vibrational frequencies and the experimental values are listed in supplementary tables 2 and 3. Here we have discussed only FTIR active modes. The experimental frequencies of Lantadene A and B and frequencies calculated by B3LYP/6-311 G (d, p) method are nearly the same. Some Important modes of vibration are discussed below.

**Table 2.** Calculated  $\epsilon_{\text{HOMO}}$ ,  $\epsilon_{\text{LUMO}}$ , energy band gap ( $\epsilon_{\text{LUMO}} - \epsilon_{\text{HOMO}}$ ), chemical potential ( $\mu$ ), electronegativity ( $\chi$ ), global hardness ( $\eta$ ), global softness ( $S$ ), and global electrophilicity index ( $\omega$ ) for compound A, B at B3LYP/6-311 G (d, p) level.

Folder	$\epsilon_{\text{H}}$	$\epsilon_{\text{L}}$	$\epsilon_{\text{H}} - \epsilon_{\text{L}}$	$\chi$	$\mu$	$\eta$	$S$	$\omega$	$\Delta N \text{ max}$
A	-0.2253	-0.0148	-0.2105	3.266	-3.266	2.863	0.1754	1.871	1.141
B	-0.2312	-0.0470	-0.1842	3.785	-3.785	2.506	0.1999	2.863	1.142

**Table 3.** Topological parameters for bonds of interacting atoms: LANTADENE-A and B electron density ( $\rho_{\text{BCP}}$ ), Laplacian of electron density ( $\nabla^2\rho_{\text{BCP}}$ ), total electron energy density ( $H_{\text{BCP}}$ ), estimated interaction energy ( $E_{\text{int}}$ ) at bond critical point (BCP).

LANT A									
Bond	$\rho_{\text{BCP}}$	$\nabla^2\rho_{\text{BCP}}$	$\left \frac{\lambda_1}{\lambda_3}\right $	$V_{\text{BCP}}$	$G_{\text{BCP}}$	$\left \frac{V(r)}{G(r)}\right $	$H_{\text{BCP}}$	$E_{\text{int}}$ (kcal/mol)	Nature
H88-O4	0.00347	0.01170	0.11970	-0.00195	0.00243	0.80247	0.00048	0.61210	VW
H73-O4	0.00456	0.01481	0.14080	-0.00264	0.00317	0.83281	0.00053	0.82800	VW
H55-H75	0.01450	0.05280	0.32110	-0.00859	0.01088	0.78952	0.00229	2.69500	W
O1-H79	0.01138	0.03972	0.13120	-0.00746	0.00869	0.85846	0.00123	2.34100	W
H71-H74	0.01288	0.04076	0.11940	-0.00677	0.00481	1.40748	-0.00196	2.12400	W
H77-H50	0.01374	0.04730	0.13020	-0.00784	0.00984	0.79675	-0.0020	2.46000	W
LANT B									
Bond	$\rho_{\text{BCP}}$	$\nabla^2\rho_{\text{BCP}}$	$\left \frac{\lambda_1}{\lambda_3}\right $	$V_{\text{BCP}}$	$G_{\text{BCP}}$	$\left \frac{V(r)}{G(r)}\right $	$H_{\text{BCP}}$	$E_{\text{int}}$ (kcal/mol)	Nature
H72-O4	0.00450	0.01470	0.13030	-0.00259	0.00310	0.83548	0.00051	0.8130	VW
H86-O5	0.01730	0.06050	0.12950	-0.01140	0.01314	0.86758	0.00174	3.5770	W
H78-O1	0.01190	0.04160	0.11820	-0.00782	0.00910	0.85934	0.00128	2.4530	W
H51-H71	0.01290	0.04410	0.12070	-0.00718	0.00911	0.78815	0.00193	2.2530	W
H54-H74	0.01420	0.05280	0.14080	-0.00859	0.00109	7.8807	-0.00750	2.6950	W
H75-H59	0.01270	0.03840	0.13210	-0.00659	0.00809	0.81459	0.00150	2.0680	W

### O-H and -CH modes of vibration

The Lantadene A and B both have hydroxyl group (-OH). In general, -OH stretching modes of vibration are observed in the range 3400–3600  $\text{cm}^{-1}$  [33]. The -OH modes of vibration appears at higher frequency region due to lower reduced mass. A significant polarized IR peak with polarization vector appears along plane appears at 3466  $\text{cm}^{-1}$  in Lantadene A with PED 100% and corresponding sharp peak superimpose in Lantadene B at 3610  $\text{cm}^{-1}$  with 100 % PED. At lower frequencies region a very intense polarized peak appears at 1018  $\text{cm}^{-1}$  in Lant A and corresponding peaks appears at 1110  $\text{cm}^{-1}$  with several mixing mode of vibrations due to in plane bending of -OH vibration. At lower frequencies region two back to back intense peaks are calculated at 591  $\text{cm}^{-1}$  and 614  $\text{cm}^{-1}$  for Lant A and 589  $\text{cm}^{-1}$ , 605  $\text{cm}^{-1}$  for Lant B due to wagging modes of -OH with mixing of several modes of vibrations too. All these calculated peaks are in good agreement with experimental FTIR.

In general, hetero aromatic geometry C-H stretching modes of vibration appears in between 2800–3100  $\text{cm}^{-1}$  [34]. In the present study, two sharp polarized peak appears at 2993 and 3002  $\text{cm}^{-1}$  with PED 95% appears due C-H stretching mode of vibration in Lantadene A and corresponding peak appears at 2993 and 3008  $\text{cm}^{-1}$  in Lantadene B with PED 99% which are also supported with literature. At lower end of frequencies in-plane and out of plane -CH bending appears. In present calculation polarized peaks appears due in plane -CH bending appears at 1298  $\text{cm}^{-1}$  in Lantadene A, however corresponding peaks appears at 1123  $\text{cm}^{-1}$  for Lantadene B with significant PED. Below 1100  $\text{cm}^{-1}$ , out of plane -CH bending mode mixing with wagging of -CH<sub>2</sub>/CH<sub>3</sub> appears at the appropriate range in the calculated spectrum for Lantadene A and B which are well matched with experimental FTIR.

### -C=O absorption vibration and C–C vibrations

The absorption bands (sharp stretching modes of vibration) of the carbonyl group (C=O) are observed in between 1600–1800  $\text{cm}^{-1}$  [35]. The intense-C=O absorption intense peaks due to stretching of both carbon and oxygen with equal amplitude. In present communication most, intense polarized peaks with polarization vector directed along plane of adjacent rings are appeared at 1640 and 1668  $\text{cm}^{-1}$  with PED 99 %, and 65 % in Lantadene A while 1695, 1711 and 1745  $\text{cm}^{-1}$  with PED of 95 %, respectively in Lantadene B.

The vibrations relating to C-C stretching in the ring absorb in the region from 1400- 1600  $\text{cm}^{-1}$  [36] in aromatic hydrocarbons. In the present calculation, intense polarized peak appears at 1102  $\text{cm}^{-1}$  due to -CC in plane bending mode of vibration in Lantadene A and stretching mode of vibration with mixed modes at 1104  $\text{cm}^{-1}$  in Lantadene B. The bending of -CCC modes appears at middle frequencies in calculated IR spectra of Lantadene A and B. At lower region of IR spectra, some intense polarized peaks are found due to out of plane bending -CH along with mixing of other bending mode for Lantadene A as well as Lantadene B. All these calculated peaks are matched well with experimental FTIR.

### Methylene(-CH<sub>2</sub>) and Methyl (-CH<sub>3</sub>) group vibrations

The CH<sub>2</sub>/CH<sub>3</sub> groups due to internal coordinate arrangement [37], having six different mode of vibration namely asymmetric, symmetric stretch, rocking, scissoring, twisting as well as wagging. In general, symmetric stretching -CH<sub>2</sub>/CH<sub>3</sub> appears middle/lower frequencies region due to weaker bond strength and characteristic region for symmetric -CH<sub>2</sub>/CH<sub>3</sub> observed in between 2800  $\text{cm}^{-1}$  to 3000  $\text{cm}^{-1}$  however antisymmetric stretching vibration for -CH<sub>2</sub>/CH<sub>3</sub> observed some higher frequencies region 3100  $\text{cm}^{-1}$ –3400  $\text{cm}^{-1}$  due to strong bond strength [38]. In the present study, the scissoring mode of deformation CH<sub>2</sub> groups shows some sharp peaks appears at 1455  $\text{cm}^{-1}$ , 1481  $\text{cm}^{-1}$  in Lantadene A however an intense polarized peak appears at 1430  $\text{cm}^{-1}$  due scissoring mode of deformation CH<sub>3</sub> groups appears in calculated spectra of Lantadene B. Some other polarized peaks appear due mixing of in plane deformation rocking due to -CH<sub>3</sub> appears at 1084  $\text{cm}^{-1}$  and 1196  $\text{cm}^{-1}$  in Lantadene B. At lower region of calculated IR spectra of Lantadene A, sharp polarized peak of -CH<sub>2</sub>/-CH<sub>3</sub> appears at 1043  $\text{cm}^{-1}$ /1211  $\text{cm}^{-1}$  while in Lantadene B, 733  $\text{cm}^{-1}$ /964  $\text{cm}^{-1}$  due to mixing of wagging with twisting modes frequencies. All these calculated peaks are in good agreement with experimental FTIR spectra.

### TDDFT analysis

The TDDFT method is utilized by using optimized geometry of Lantadene A and Lantadene B molecule to calculate UV spectrum. The calculated transition state and transition orbital and their %

contribution, Transition energy, oscillatory strength  $\lambda_{\max}$ , are calculated and listed in table 1. The UV spectra of Lantadene A and Lantadene B are shown in Fig. 3. In Fig. 3, the green vertical lines are showing the peaks of calculated wave length in graph having greater oscillatory strength. From this figure a prominent peak appears at 258 nm with  $f=0.0005$  in Lantadene A while 259 and 291 nm with  $f=0.0003$  for both wave length in Lantadene B respectively. The transition energy of electron is 4.81 eV and 4.79/4.26 eV in Lantadene A and Lantadene B respectively. The peak emerges due to transition of electron in between HOMO -4 $\rightarrow$ LUMO with contribution of 80 % in Lantadene A while HOMO-4 $\rightarrow$ LUMO/ HOMO-1 $\rightarrow$ LUMO+1 with contribution of 92 %/95 % in Lantadene B. Two other less sharp peak appears at 291nm ( $f=0.0003$ ) and 263nm (0.0002) in Lantadene A while one at 270 nm ( $f=0.0002$ ) in Lantadene B. The calculated transition energy corresponds to these transitions at 4.26/4.71 eV for Lantadene A while 4.59 eV for Lantadene B.

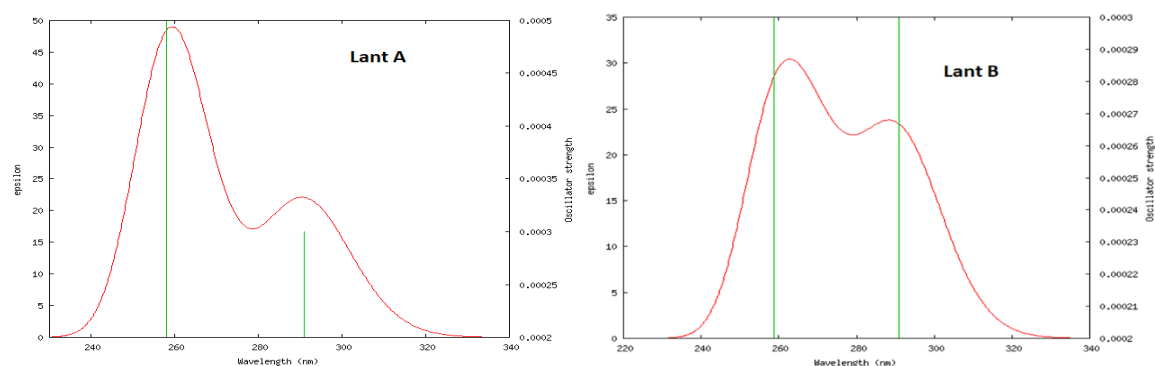


Fig. 3. UV spectrum of Lantadene A and B.

### Electronic properties (HOMO-LUMO, MESP Plots of Lantadene A and Lantadene B)

The chemical reactivity or chemical stability is determined by frontier molecular orbitals (FMO). In FMO, the highest occupied molecular orbital is termed as HOMO and lowest unoccupied molecular orbital is termed as LUMO. The supplied energy to transition of electron from HOMO to LUMO is known forbidden energy band gap. The energy gap is directly related with chemical stability [39-40]. The calculated energy gap shows that chemical reactivity of Lantadene A (5.7256 eV) is little bit less than Lantadene B (5.0102 eV). The HOMO and LUMO plots of Lantadene A and Lantadene B are shown in Fig. 4(a) and 4(b). The HOMO of Lant A is distributed over Ring C and associated group and LUMO is nearly over ring E. The HOMO of Lant B is distributed over Ring C and associated group and LUMO is nearly over ring E. The transition from HOMO $\rightarrow$ LUMO shows that electron transfer from Ring C and associated group to ring E to gain stability in both molecules.

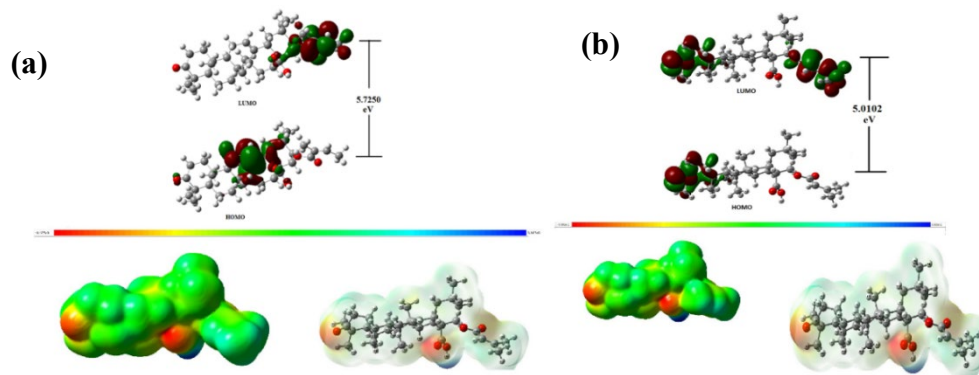


Fig. 4. (a) Pictures of HOMO-LUMO and Molecular Electrostatic Potential of Lantadene A, (b) Pictures of HOMO-LUMO and Molecular Electrostatic Potential of Lantadene B.

The ionization potential and electron affinity are any chemical system is determined by HOMO and LUMO energy. The energy needed to remove one electron from HOMO orbital is known as electronic potential and energy needed to add additional electron in LUMO is known as electron affinity. The Parr et.al [41], suggest that negative eigen value of HOMO is called ionization potential (IP) however negative eigen value of LUMO is called electron affinity (EA).

$$IP = -\text{HOMO} \quad (1)$$

$$EA = -\text{LUMO} \quad (2)$$

By using EA and IP chemical hardness and absolute electronegativity are determined by using following equations [42, 43],

$$\mu = -(\text{IP} + \text{EA})/2 \quad (3)$$

$$\eta = (\text{IP} - \text{EA})/2 \quad (4)$$

The calculated value of energy gap implies that Lantadene B is more chemically reactive than Lantadene A. The electron affinity of Lantadene B is more than Lantadene A, this implies that Lantadene B have better tendency to gain additional electron to gain stability which is also reflect calculated value of chemical potential of both species. The calculated chemical hardness of Lantadene A is higher than Lantadene B. This means that any reagent easily interacts with Lantadene B rather than Lantadene A. The chemical softness implies that how easily any reagent interacts with given species and shows reverse effect with chemical hardness. The reciprocal of chemical hardness is termed as the global softness,

$$S = 1/2\eta \quad (5)$$

[44-45]

The calculated value  $N_{\text{max}}$  is ratio of chemical potential and chemical hardness and show direction of charge transport to gain stability. All these parameters are listed in table 2.

$$(\Delta N_{\text{max}})_I = -\frac{\mu_I}{\eta_I} \quad (6)$$

The direction charge transport is determined by magnitude of chemical potential due to electrophilic species is accomplished to receive charge from donor atom consequently system get stabilized and attend lower energy.

The electrophilicity index is a global reactivity descriptor of a molecule that provides a quantitative classification of the global electrophilic nature of the molecule. The chemical potential of a species in a mixture can be defined as the slope of the free energy of the system with respect to a change in the number of moles of that species. It is a form of potential energy that can be absorbed or released during a chemical reaction. Although electronegativity is defined in many different ways, the most logical and rational definition of it is the electron holding power of the atoms or molecules.

The molecular electrostatic energy potential plot is very important picture to determine nature of potential of atomic sites within the molecule. The nature of electron potential surface is determined in term of color coding. The consequence of MESP lies in the detail that it concurrently displays molecular size, shape, and positive, negative, and neutral electrostatic potential regions in terms of color grading example yellow color means neutral potential surface blue color shows electropositive surface and red color as electronegative surface [46-49]. The MESP plots of Lantadene A and B are also shown on Fig. 4(a) and 4(b). From this figure, red color encircled over  $-\text{COO}-\text{C}_2\text{H}_5\text{CH}_3$  group and over  $-\text{COOH}-$  and  $-\text{CO}$  of ring A in Lant A and Lant B respectively so behaves as most electronegative surface in Lant A and Lant B. In both Lant A and Lant B, blue

color encircled over -OH in -CH<sub>2</sub>OH group attached at ring D and E. The white color encircled over whole molecule in Lant A and Lant B.

### QATIM analysis

The quantum atomic theory in molecule QAIM [50] is significant tool to determine nature and strength of nonbonding or bonding interactions by using topological parameters. The bond critical point is known as four critical point (3,-1) is introduced by Bader which provides information to define interactions like covalent and non-covalent interaction in any chemical system. The nature and strength of non-covalent interaction are calculated by some topological parameters e.g. electron density  $\rho(r)$ , local potential energy density  $V(r)$ , Laplacian  $\Delta^2 \rho(r)$ , Total energy density  $H(r)=V(r)+G(r)$ , etc. The topological parameters at bond critical point (BCP) for Lant A and Lant B are calculated and listed in table-3 respectively. The graphical AIM pictures of interactions for Lant A Lant B are shown in Fig. 5. The electron density ( $\rho_{H...A}$ ) falls in between 0.002–0.040 a.u. and Laplacian ( $\nabla^2 \rho_{BCP}$ ) falls in between 0.024–0.139 a.u. for nonbonding interactions [51]. Based on these criteria of nonbonding six nonbonding interactions appear in both Lant A and Lant B for nonbonding. In Lant A molecule six nonbonding interactions are H<sub>88</sub>-O<sub>4</sub>, H<sub>73</sub>-O<sub>4</sub>, H<sub>55</sub>-H<sub>75</sub>, O<sub>1</sub>-H<sub>79</sub>, H<sub>71</sub>-H<sub>74</sub>, H<sub>77</sub>-H<sub>50</sub> however in Lant B corresponding interactions are H<sub>72</sub>-O<sub>4</sub>, H<sub>86</sub>-O<sub>5</sub>, H<sub>78</sub>-O<sub>1</sub>, H<sub>51</sub>-H<sub>71</sub>, H<sub>54</sub>-H<sub>74</sub>, H<sub>75</sub>-H<sub>59</sub>. The charge density  $\rho_{BCP}$  at BCP in Lant A varies from 0.00347a.u.-0.01450a.u. and got its maximum for H<sub>55</sub>-H<sub>75</sub> and minimum value for H<sub>88</sub>-O<sub>4</sub> however charge density at BCP for Lant B varies in between 0.00450 a.u.-0.01420a.u. The maximum value of  $\rho_{BCP}$  for H<sub>54</sub>-H<sub>74</sub> and minimum value of  $\rho_{BCP}$  for H<sub>72</sub>-O<sub>4</sub>. The charge density at BCP for O-H interaction varies in between 0.00450- 0.01190 a.u. in Lant B and 0.00347-0.01138 a.u. in Lant A. From this data,  $\rho_{BCP}$  for O-H interaction for LantB > LantA. The calculated  $\rho_{BCP}$  for H-H interaction 0.01288-0.01450 a.u. in Lant A and corresponding charge density for H-H interaction in Lant B varies in between 0.01270 to 0.01420. One important thing noticed  $\rho_{BCP}$  for H-H interaction >O-H interaction. For both Lant A and Lant B order of magnitude of charge density  $\rho(r)$  are smaller as compared with typical covalent bond but lesser value of  $\rho(r)$  between these interactions for O-H in both Lant A Lant are comparable with to 0.007 au in HCl---HF [52]. The second derivative of laplacian charge density ( $\nabla^2 \rho_{BCP}$ ) for Lant A varies from 0.01170 to 0.05280 a.u. and attained maximum value  $\nabla^2 \rho_{BCP} = 0.05280$ a.u. for H<sub>55</sub>-H<sub>75</sub> however Laplacian second derivatives of electron charge density varies from 0.01470 -0.05280 for Lant B and attained maximum value for  $\nabla^2 \rho_{BCP} = 0.05280$  a.u. for H<sub>54</sub>-H<sub>74</sub>. The existence of small delocalization between both interacting atoms shown by using calculated  $\nabla^2 \rho_{BCP}$  in both natural products. In both natural product Lant A and Lant B for all six interactions  $\nabla^2 \rho_{BCP} > 0$  and  $\rho_{BCP} > 0$  means all interaction are electrovalent nature. The sign of Laplacian electron density  $\nabla^2 \rho_{BCP}$  shows that concentration of charge in a exhausted or “closed shell. In Lant A for all six interaction  $\nabla^2 \rho_{BCP} > 0$  and  $\rho_{BCP}$  lies within range  $10^{-3}$  for H<sub>73</sub>-O<sub>4</sub>, H<sub>88</sub>-O<sub>4</sub> for Lant A and H<sub>72</sub>-O<sub>4</sub> for Lant B falls within van der Waals ‘interaction [53]. The rest all interaction in both Lant A and Lant B  $\rho_{BCP}$  lies within range  $10^{-2}$  and falls within hydrogen bonding interactions [54]. The calculated potential energy density at BCP are determine nature and strength of interactions. The nonbonding at BCP is weak when  $\nabla^2 \rho_{BCP} > 0$ , HBCP > 0 and interaction is called electrovalent for  $\nabla^2 \rho_{BCP} > 0$ , HBCP < 0. The all interactions in both Lant A and Lant B are weak except H<sub>77</sub>-H<sub>50</sub> H<sub>71</sub>-H<sub>74</sub> for Lant A H<sub>54</sub>-H<sub>74</sub> for Lant B falls in electrovalent category. The interactions in between atoms are calculated by following equation  $\Delta E = -1/2V$  [55]. All interactions are falls within weak interaction lies within range 1kcal/mol < IE < 5 kcal/mol except H<sub>88</sub>-O<sub>4</sub>, H<sub>73</sub>-O<sub>4</sub> for Lant A H<sub>72</sub>-O<sub>4</sub> in Lant B lies IE < 1 kcal/mol falls very weak type interaction [56]. The strongest interaction appears for H<sub>55</sub>-H<sub>75</sub> in Lant A and H<sub>86</sub>-O<sub>5</sub> Lant B. The chemical natures of any chemical systems are calculated by using curvature point of second derivative of electron density  $\nabla^2 \rho_{BCP}$  at BCP  $\lambda_1, \lambda_2, \lambda_3$ . One of another parameter's ratio  $\left| \frac{\lambda_1}{\lambda_3} \right|$  is useful to calculate nature and types of chemical bond. [57]. All six interactions indicative of weak CSIs in Lant A and Lant B because for all six interactions  $\left| \frac{\lambda_1}{\lambda_3} \right| \ll 1$ . The ratio  $\left| \frac{V(r)}{G(r)} \right|$  is important indicator to know about nature of interaction. For all interaction  $|V(r)|/G(r) < 1$  in both Lant A and Lant B except H<sub>71</sub>-H<sub>74</sub> for Lant A H<sub>54</sub>-H<sub>74</sub> for Lant B where  $|V(r)|/G(r) > 1$  so all five interactions in both Lant A, Lant B are characteristic of hydrogen bonding, ionic, and van der Waals interaction however H<sub>71</sub>-H<sub>74</sub> for Lant A H<sub>54</sub>-H<sub>74</sub> for Lant B interaction are covalent.

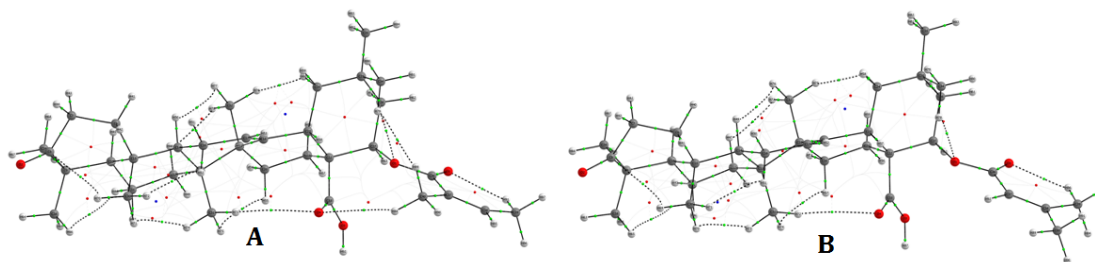


**Fig. 5.** AIM picture of Lantadene A and B representing hydrogen interaction (dotted line) with Green points and red points represent as BCPs and RCP.

### NBO analysis

The NBO analysis is important method to calculate charge transfer from donor to acceptor to determine interaction in any molecular systems [58]. The strength of interaction in term of charge transfer from donor to acceptor is determine by second order perturbation energy  $E^{(2)}$ . The strength of interaction among electron donors and electron acceptors are directly related by second order perturbation energy of  $E^{(2)}$  means the strength of interaction increases with second order perturbation energy of  $E^{(2)}$ . The strength of interaction is calculated by (or stabilization energy) [59-60]

$$E^{(2)} = -q_i \frac{(F_{ij})^2}{\epsilon_j - \epsilon_i} \quad (7)$$

In this equation population of donor orbital is  $q_i$  however orbital energies (diagonal elements) of donor are  $\epsilon_i$ ,  $\epsilon_j$ . The fock matrix donor acceptor orbitals and their occupancies as well as second-order perturbation energy of Lant A and Lant B is calculated and listed in table 4 by using same level theory. They stabilizes the system due to charge transfer in between donor and acceptor orbital overlap  $Lp \rightarrow \pi^*/\sigma^*$ . In first type of interaction  $Lp \rightarrow \sigma^*$  appears due to charge transfer in between  $Lp(2)O_5 \rightarrow \sigma^*(C_{36}-C_{37})$  orbitals stabilized system by 16.54kcal/mol and 16.40 kcal/mol for Lant A and Lant B respectively which further enhance charge transfer from  $Lp(2)O_5 \rightarrow \sigma^*(C_{36}-O_1)$  is stabilized by 32.11kcal/mol and 32.57kcal/mol in Lant A and Lant B respectively. Another significant interaction appears due to charge transfer  $Lp(2)O_4 \rightarrow \sigma^*(C_{22}-C_{33})$  which stabilized by 18.84kcal/mol and 19.10kcal/mol for Lant A and Lant B respectively. This strength of interaction  $Lp(2)O_4 \rightarrow \sigma^*(O_3-C_{33})$  further enhance by 31.07kcal/mol and 33.49kcal/mol in Lant A and Lant B respectively. The significant interaction appears in between  $Lp(2)O_2 \rightarrow \sigma^*(C_8-C_9)$  stabilize by 9.81kcal/mol and 20.43kcal/mol for Lant A and Lant B respectively which further enhance in interactions  $Lp(2)O_2 \rightarrow \sigma^*(C_7-C_8)$  by 19.82kcal/mol and 20.21kcal/mol for Lant A and Lant B respectively. In second type interaction one important interactions happens in among  $Lp(2)O_3 \rightarrow \pi^*(O_4-C_{33})$  which stabilize by 43.40kcal/mol and 43.57kcal/mol for Lant A and Lant B respectively. Another important interaction appears in between  $Lp(2)O_1 \rightarrow \pi^*(O_5-C_{36})$  which stabilize Lant A and Lant B by 42.81kcal/mol and 42.61kcal/mol respectively.

**Table-4.** NBO analysis of donor acceptor orbitals and their occupancies second order perturbation interaction energy for Lant A and Lant B

LANT-A						
Donor NBO( <i>i</i> )	occupancy( <i>i</i> )	Acceptor NBO( <i>j</i> )	occupancy( <i>j</i> )	$E^{(2)}$ (kcal/mol)	$(E_j - E_i)$ a.u	$F(i,j)$ a.u
Lp(2)O <sub>5</sub>	1.84332	$\sigma^*(C_{36}-C_{37})$	0.0669	16.54	0.69	0.097
Lp(2)O <sub>5</sub>	1.84332	$\sigma^*(C_{36}-O_1)$	0.1121	32.11	0.62	0.127

Lp(2)O <sub>4</sub>	1.85624	σ*(C <sub>22</sub> -C <sub>33</sub> )	0.0724	18.84	0.63	0.099
Lp(2)O <sub>4</sub>	1.85624	σ*(O <sub>3</sub> -C <sub>33</sub> )	0.0941	31.07	0.61	0.125
Lp(2)O <sub>3</sub>	1.82363	π*(O <sub>4</sub> -C <sub>33</sub> )	0.0210	43.40	0.34	0.109
Lp(2)O <sub>2</sub>	1.89039	σ*(C <sub>8</sub> -C <sub>9</sub> )	0.0778	19.81	0.65	0.102
Lp(2)O <sub>2</sub>	1.89039	σ*(C <sub>7</sub> -C <sub>8</sub> )	0.0618	19.82	0.66	0.103
Lp(2)O <sub>1</sub>	1.79238	π*(O <sub>5</sub> -C <sub>36</sub> )	0.2002	42.81	0.34	0.108
<b>LANT-B</b>						
Donor NBO(i)	occupancy(i)	Acceptor NBO(j)	occupancy(j)	E <sup>(2)</sup> (kcal/mol)	(E <sub>j</sub> -E <sub>i</sub> ) a.u	F(i,j) a.u
Lp(2)O <sub>5</sub>	1.84493	σ*(C <sub>36</sub> -C <sub>37</sub> )	0.1025	16.40	0.70	0.098
Lp(2)O <sub>5</sub>	1.84493	σ*(C <sub>36</sub> -O <sub>1</sub> )	0.1025	32.57	0.62	0.129
Lp(2)O <sub>4</sub>	1.84347	σ*(C <sub>22</sub> -C <sub>33</sub> )	0.0769	19.10	0.63	0.100
Lp(2)O <sub>4</sub>	1.84347	σ*(O <sub>3</sub> -C <sub>33</sub> )	0.1017	33.49	0.61	0.129
Lp(2)O <sub>3</sub>	1.82589	π*(O <sub>4</sub> -C <sub>33</sub> )	0.0224	43.57	0.35	0.111
Lp(2)O <sub>2</sub>	1.88771	σ*(C <sub>8</sub> -C <sub>9</sub> )	0.0788	20.43	0.65	0.104
Lp(2)O <sub>2</sub>	1.88771	σ*(C <sub>7</sub> -C <sub>8</sub> )	0.0613	20.21	0.67	0.105
Lp(2)O <sub>1</sub>	1.79787	π*(O <sub>5</sub> -C <sub>36</sub> )	0.0223	42.61	0.34	0.109

### NLO properties

The nonlinear optical properties NLO of Lant A and Lant B are calculated by using several parameters like dipole moment, mean polarizability, anisotropic polarizability, molar refractivity (MR) hyperpolarizability etc. In three dimensional Cartesian coordinate system dipole moment, mean polarizability, hyperpolarizability are calculated by using following equation [61]

$$\mu = (\mu_x^2 + \mu_y^2 + \mu_z^2)^{1/2} \quad (8)$$

$$\langle \alpha \rangle = 1/3 [\alpha_{xx} + \alpha_{yy} + \alpha_{zz}] \quad (9)$$

$$\beta_{\text{Total}} = (\beta^2_x + \beta^2_y + \beta^2_z)^{1/2} = [(\beta_{xxx} + \beta_{xyy} + \beta_{xzz})^2 + (\beta_{yyy} + \beta_{yxx} + \beta_{yzz})^2 + (\beta_{zzz} + \beta_{zxx} + \beta_{zyy})^2]^{1/2} \quad (10)$$

The hyperpolarizability ( $\beta$ ), a nonlinear-optical property of a molecule, is the second-order electric susceptibility per unit volume. The electric susceptibility is a dimensionless proportionality constant that indicates the degree of polarization of a dielectric material in response to an applied electric field. The greater the electric susceptibility, the greater the ability of a material to polarize in response to the field, and thereby reduce the total electric field inside the material (and store energy). It is in this way that the electric susceptibility influences the electric permittivity of the material.

$$\Delta\alpha = \left[ \frac{(\alpha_{xx} - \alpha_{yy})^2 + (\alpha_{yy} - \alpha_{zz})^2 + (\alpha_{zz} - \alpha_{xx})^2}{2} \right]^{1/2} \quad (11)$$

The Lorenz-Lorentz are used by using molar refractive index [62-64]

$$MR = \left[ \frac{n^2 - 1}{n^2 + 2} \right] \left( \frac{MR}{\rho} \right) = 1.33\alpha\pi N \quad (12)$$

In this equation,  $\alpha$  is the mean polarizability and  $N$  is the Avogadro number. The polarizability ( $\alpha_e$ ) along x axis and polarizability along y axis is ( $\alpha_o$ ). By using these polarizability ordered parameter is computed by following equation [65-66]

$$S = \frac{\alpha_e - \alpha_o}{\alpha_e + \alpha_o} \quad (13)$$

(For  $\alpha$ : 1 a.u. =  $0.1482 \times 10^{-24}$  esu; for  $\beta_0$ : 1 a.u. =  $8.639 \times 10^{-33}$  esu)

The dipole moment of any system is signature of magnitude charge distribution on any that system without application electric field. The calculated dipole moment of Lant A and Lant B are nearly 1.5 times of dipole moment of water (1.85D). This large dipole moment reported due to unsymmetrical distribution of title molecules with unequal electronegative atoms like oxygen hydrogen and carbon however calculated dipole moment of Lant B > Lant A molecule. The polarizability as well as well hyperpolarizability of any system are described by applied electric field. The mean polarizability, hyperpolarizability, molar refractivity (MR), order parameters. Anisotropic polarizability, of Lant A and Lant B are calculated and listed in table 5. The greater calculated mean polarizability anisotropic polarizability based on direction molar refractivity (MR) for Lant B established superiority over NLO properties for Lant A molecule. The calculated order parameters for both Lant A and Lant B are still lower as compared with established NLO materials but order parameter for Lant A is greater than Lant B. The calculated hyperpolarizability of Lant B Lant A are nearly six times greater than corresponding value of reference molecule urea ( $0.1947 \times 10^{-30}$  e.s.u.) however calculated hyperpolarizability of Lant B is greater than Lant A. The NLO activity appears on Lant A and Lant B due moment of  $\pi$  electron from donor to acceptor in both Lant A and Lant B.

**Table 5.** Polarizability and Hyper Polarizability of Lant A and Lant B.

Species	$\langle \alpha \rangle$ (a.u.)	$\Delta \alpha$ (a.u.)	MR (e.s.u.)	S	Cos $\phi$	$\beta_{total}$ (a.u.)	$\mu$ (D)
Lant A	394.4213	162.8472	147.1586	0.19350	0.46233	120.7553	3.123
Lant B	397.3975	163.678	148.269	0.193138	0.46209	124.4178	3.427

## Molecular docking

The molecular docking indicates binding action of drug with appropriate protein. The docking action of Lant A and Lant B with selected protein has been performed by Auto Dock 4.2 software [67]. In docking process grid of  $60 \text{ \AA} \times 60 \text{ \AA} \times 60 \text{ \AA}$  size was selected for docking. In preparation process of protein, we removed co-crystallized ligands and water molecules from selected PDB file. By using UCSF Chimera program [68] Gasteiger charges as well as hydrogen atoms were allocated to protein residues. The Lant A and Lant B were docked with prepared protein by using Auto Dock 4.2 program package which consider Lamarckian Genetic Algorithm (LGA) [69]. The Discovery Studio software [70] utilized for visualization of interactions between Lant A and Lant B with suitable protein.

The appropriate targets are calculated by using Swiss dock is online server [71]. The swiss dock online server predicts three proteins for docking with Lant A and Lant B molecule. The Swiss dock is online server which based on newton mechanics utilized to predict target protein for docking. In target prediction by swiss dock online server we have uploaded optimized geometry of LantA and Lant B uploaded smile code of optimized geometry on swissdock server. The docking of the proteins of all structures of BCL2L1 and IKBKB with participating atoms of Lant A and Lant B and corresponding bond lengths are listed in tables 6 and 7 and all possible interaction during docking were presented by LIGPLOT. The binding affinity is closely related with number of atoms in ligand so ligand efficiency index of title molecule with respect to particular targets. The

ligand efficiency is designed separating the score found in the docking simulation by the total number of non-hydrogen atoms of the ligand.

**Table 6.** Different parameters for molecular docking of Lant A and B with different protein structures.

Target Proteins	Selected PDB structures with their resolutions	Hydrogen Bonding residues		Ligand efficiency		Inhibition constant ( $\mu$ M)		Binding energy (kcal/mol)	
		Lant A	Lant B	Lant A	Lant B	Lant A	Lant B	Lant A	Lant B
<b>BCL2L1</b> <b>BCL2</b> like 1provided by HGNC	6WGZ 2.20 Å	TRPA:140 GLUA:326	ASNA:140	0.1475	0.1675	74.3354	75.09123	-5.9	-6.7
	6WH0 1.99 Å	TYRA:29	LYSA:355	0.1525	0.1625	23.5650	27.2025	-6.1	-6.5
	202M 2.25 Å	ASNA:140 GLYA142	ASNA:140	0.1275	0.1450	124.9156	124.8355	-5.1	-5.8
<b>IKBKB</b> inhibitor of nuclear factor kappa B kinase subunit beta	4kik 2.83 Å	LIUB:21 LYSB:147 TRYB:98	CYSB:99	0.1475	0.1350	107.8772	109.2227	-5.9	-5.4
	3rzf 4.0 Å	ASNA:140 GLYA:142	ASPA:103 GLYA:102 LYSA:106	0.1575	0.1800	80.8633	81.0748	-6.3	-7.2

**Table 7.** Hydrogen bonding residues, Binding atoms and Bond length for molecular docking of Lant A and B with different protein structures.

Target Proteins	Selected PDB structures with their resolutions	Hydrogen Bonding residues		Binding atoms		Bond length	
		Lant A	Lant B	Lant A	Lant B	Lant A	Lant B
<b>BCL2L1</b> <b>BCL2</b> like 1provided by HGNC	6WGZ 2.20 Å <sup>0</sup>	TRPA:140 GLUA:326	ASNA:140	O3 O2	O5	2.319 2.132	2.103
	6WH0 1.99 Å <sup>0</sup>	TYRA:29	LYSA:355	O2	O5	1.419	1.813
	202M 2.25 Å <sup>0</sup>	ASNA:140 GLYA142	ASNA:140	O3 O5	O2	2.464 2.032	2.723
<b>IKBKB</b> inhibitor of nuclear factor kappa B kinase subunit beta	4kik 2.83 Å <sup>0</sup>	LIUB:21 LYSB:147 TRYB:98	CYSB:99	O3 O2 O5	O3	1.976 1.945 1.932	2.221
	3rzf 4.0Å <sup>0</sup>	ASNA:140 GLYA:142	ASPA:103 GLYA:102 LYSA:106	O5 O3	O3 O1 O5	2.255 2.469	2.421 2.221 2.404





80.8633  $\mu\text{M}$  and 81.0784  $\mu\text{M}$  respectively for Lant A and Lant B which lies corresponding lower value for 4kik structure. The other pdb geometry 4kik of IKBKB loosely binds with residues. The docking of these selected geometries with Lant A and Lant B are shown in Figures 6(a) and 6(b) and 7(a) and 7(b).

## Conclusions

Our study delves into the characterization of Lantadene A and B through FTIR spectroscopy, employing the B3LYP/6-311G (d, p) method to calculate their fundamental vibrational frequencies. A comprehensive assignment of vibrational wavenumbers has been achieved through potential energy distribution (PED) analysis, demonstrating an impressive concordance between our calculated spectra and experimental observations. Additionally, to substantiate our findings, we conducted TDDFT calculations. In our quest to illustrate the reactivity of Lantadene A and B, we computed several chemical parameters, including the HOMO-LUMO gap. We further visualized their frontier orbitals, HOMO-LUMO surfaces, and Molecular Electrostatic Potential (MEP) surfaces, shedding light on their inherent reactivity. Furthermore, our investigation into hyperpolarizability values suggests the potential utility of these compounds in electro-optical applications. We also explored the molecular docking interactions of Lantadene A and B with suitable protein targets, offering a detailed analysis of the results. Our findings suggest that these compounds hold promise as candidates for anticancer and anti-inflammatory applications. In summary, our study underscores the potential of Lantadene A and B in the realms of both molecular reactivity and therapeutic applications, particularly in the context of anticancer and anti-inflammatory agents, while also highlighting their suitability for electro-optical endeavors.

## Acknowledgements

One of the authors Anoop Kumar Pandey is grateful and thanks the Uttar Pradesh government (India) [No: 46/2021/603/sattar-4-2021-4(56)/2020] for providing him financial support. V.S. thanks the CHPC Lengau, South Africa, for the computational facility.

## References

1. Nadkarni, A.K., Nadkarni, K.M., *Indian Materia Medica*, Bombay Popular Prakashan, Bombay, 1976.
2. Guthikonda, R.N., Cama, L.D., Quesada, M., Woods, M.F., Salzmann, T.N., Christensen, B.G., *Pure & Appl. Chem.* **1987**, 3, 455-458. DOI: <http://dx.doi.org/10.1351/pac198759030455>.
3. Ross, I. A., *Medicinal plants of the world*, Human Press, New Jersey, 1999. DOI: <https://doi.org/10.1007/978-1-59259-365-1>.
4. Kurian, A., K, Shankar M., *Medicinal Plants-Horticulture Sciences*, New India Publication Agency, India, 2007.
5. The Wealth of India. The Council of Scientific and Industrial Research, *Ind Med Gaz.* **1949**, 84(10), 476-477. PMID: PMC5189551.
6. Vasantha, P., Sukumar, N., Sharma, O. P., *Acta Cryst.* **1991**, C47, 810-812.
7. Ghisalberti, E.L., *Fitoterapia*, **2000**, 71, 467-485. DOI: [http://doi.org/10.1016/S0367-326X\(00\)00202-1](http://doi.org/10.1016/S0367-326X(00)00202-1)
8. Duke, J. A., Boca Raton, *CRC Press*, 1992.
9. Shashi, B.M., Niranjan, P.S., Subodh, K.R., Sharma, O.P., *Tetrahedron*, **1994**, 50, 9439-9446. DOI: [http://doi.org/10.1016/S0040-4020\(01\)85518-6](http://doi.org/10.1016/S0040-4020(01)85518-6).

10. O' Neill, M.J., Lewis, J.A., Noble, H.M., Holland, S., Mansat, C., Farthing, J.E., Foster, G., Noble, D., Lane, S.J., Sidebottom, P.J., Lynn, S.M., Hayes, M.V., Dix, C.J., *J. Nat. Prod.*, **1998**, 61, 1328- 1331. DOI: <http://doi.org/10.1021/np970464j>.
11. Uzcategui, B., Avila, D., Heberto, S.R., Quintero, L., Ortega, J., Gonzalez, Y.B., *Investigacion Clinica*, **2004**, 45, 4.
12. Misra, N., Sharma, M., Raj K., Dangi, A., Srivastava, S., Misra, S., *Parasitol. Res.*, **2007**, 100, 439-448. DOI: <http://doi.org/10.1007/s00436-006-0312-y>.
13. Begum, S., Wahab, A., Siddiqui, B., Qamar, F., *Chem. Pharm. Bull.* **2003**, 51, 134–137. DOI: <http://doi.org/10.1248/cpb.51.134>.
14. Zandi-Sohani, N., Hojjati, M., Carbonell, B., Angel, A., *Chil. J. Agric. Res.*, **2012**, 72, 502-506. DOI: <http://dx.doi.org/10.4067/S0718-58392012000400007>
15. Shamsi, Z. R., Al-Saffar, A.Z., Al-Shanon, A.F., Al-Obaidi, J.R., *Mol. Biol. Rep.*, **2019**, 46, 381-390. DOI: <http://doi.org/10.1007/s11033-018-4482-3>.
16. Inada, Nakanishi, T., Tokuda, H., Nishino, H., Iwashina, A., and Sharma, O. P., *Planta. Med.*, **1995**, 61, 558.
17. Inada, Nakanishi, T., Tokuda, H., Nishino, H., Iwashina, A., and Sharma, O. P., *Planta. Med.*, **1997**, 63, 272.
18. Nethaji, M., Rufes, C., Sadasivao, C., Pattashi, V. Sharma, O., *J. Crystallogr. Spectrosc. Res.*, **1993**, 6, 469 472.
19. Goswami, G. A., Sawant, N., *Biosci. Biotechnol. Res. Asia*, **2011**, 2, 821-824. <https://www.biotech-asia.org/?p=9684>.
20. Sharma, M., Sharma, P., Bansal, M., *Indian J. Pharmacol.*, **2007**, 39,140-144.
21. Sharma, M., Dalal, R. Sharma, N, *Design Nat. Prod. Res.*, **2011**, 4, 387-396. DOI: <http://doi.org/10.1080/14786411003792173>.
22. Dwivedi, A., Srivastava, A. K., Bajpai, A., *Spectrochim. Acta, Part A.*, **2015**, 149, 343-351. DOI: <https://doi.org/10.1016/j.saa.2015.04.042>.
23. Dwivedi, A., Pandey, A. K., Raj, K., Misra, N., *Spectrosc. Int. J.*, **2012**, 3, 155-166. DOI: <http://doi.org/10.1155/2012/486304>.
24. Pandey, A. K., Siddiqui, S. A., Dwivedi, A., Raj, K., Misra, N., *Spectrosc. Int. J.*, **2011**, 25, 287-302. DOI: <http://doi.org/10.3233/SPE-2011-0517>.
25. A. K. Pandey, A. Dwivedi, N. Misra, *Spectrosc. Int. J.*, **2013**. Article ID 937915, 11 pages. DOI: <https://doi.org/10.1155/2013/937915>.
26. Dwivedi, A., Kumar, A. *Polycyclic Aromat. Compd.*, **2021**, 41, 387-399. DOI: <https://doi.org/10.1080/10406638.2019.1591466>.
27. Becke, A.D., *J. Chem. Phys.*, **1993**, 98, 5648-5652. DOI: <https://doi.org/10.1063/1.464913>.
28. Lee, C., Yang, W., Parr, R.G. *Phys. Rev. B.*, **1988**, 37, 785. DOI: <https://doi.org/10.1103/PhysRevB.37.785>.
29. Frisch, M. J., et al *Gaussian 09*; Gaussian, Inc., Pittsburgh, PA, 2009.
30. Fast, P.L., Corchado, J., Sanches, M.L., Truhlar D.G., *J. Phys.Chem. A.* **1999**, 103, 3139-3143. DOI: <https://doi.org/10.1021/jp9900382>.
31. Frisch, A., Nelson, A.B., Holder, A.J., *Gauss view*, Inc.Pittsburgh PA, 2000.
32. Jamroz M. H., *Vibrational Energy Distribution Analysis: VEDA 4 program*, Warsaw (2004).
33. Andersson, M.P., Uvdal, P. *J. Phys. Chem. A.* **2005**, 12, 2937–2941. DOI: <https://doi.org/10.1021/jp045733a>.
34. Colthup, N.B., Daly, L.H., Wiberley, S.E., *Introduction to Infrared and Raman Spectroscopy*, Academic Press, New York, 1990.

35. Abraham, C.S., Muthu, S., Prasana, J.C., Armaković, S., Armaković, S.J., Geoffrey B., *Spectrochim. Acta, Part A*, **2019**, 222, 117188. DOI: <https://doi.org/10.1016/j.saa.2019.117188>.
36. Thamarai, A., Vadamar, R., Raja, M., Muthu, S., Narayana, B., Ramesh, P., R. Muhamed, R., Sevvanthi, S., Aayisha, S., *Spectrochim. Acta, Part A*, **2020**, 226, 117609. DOI: <https://doi.org/10.1016/j.saa.2019.117609>.
37. Silverstein, R.M., Bassler, G.C., Morrill, T.C., *Spectrometric Identification of Organic Compounds*, 4th ed. John Wiley and Sons, New York, 1981.
38. Pulay, P., Fogarasi, G., Pang, F., Boggs, J.E., *J. Am. Chem. Soc.*, **1979**, 101, 2550–2560. DOI: <https://doi.org/10.1021/ja00504a009>.
39. Gutowski, M., Chalasinski, G., *J. Chem. Phys.* **1993**, 98, 4540–4554.
40. Bose, S. C., Saleem, H., Erdogdu, Y., Rajarajan, G., Thanikachalam, V., *Spectrochim. Acta, Part A*, **2011**, 82, 260–269. DOI: <https://doi.org/10.1016/j.saa.2011.07.046>.
41. Parr, R. G., Pearson, R.G., *J. Am. Chem. Soc.* **1983**, 105, 7512–7516. DOI: <https://doi.org/10.1021/ja00364a005>.
42. Geerlings, P., Proft, F. D., Langenaeker, W., *Chem. Rev.* **2003**, 103, 1793–1874. DOI: <https://doi.org/10.1021/cr990029p>
43. Parr, R.G., Donnelly, R.A., Levy, M., Palke, W.E., *J. Chem. Phys.*, **1978**, 68, 3801. DOI: <https://doi.org/10.1063/1.436185>.
44. Komorowski, L., *Chem. Phys.*, **1987**, 114, 55.
45. Parr, R.G., Szentpály, L., Liu, S., *J. Am. Chem. Soc.*, **1999**, 121, 1922–1924.
46. Gadre, S.R., Pathak, R.K., *J. Chem. Phys.*, **1990**, 93, 1770–1774. DOI: <https://doi.org/10.1063/1.459703>.
47. Gadre, S.R., Shrivastava, I.H., *J. Chem. Phys.*, **1991**, 94, 4384–4390. DOI: <https://doi.org/10.1063/1.460625>.
48. Murray J.S., Sen, K., *Molecular Electrostatic Potentials, Concepts and Applications*, Elsevier, Amsterdam, 1996.
49. Alkorta I., Perez, J.J., *Int. J. Quant. Chem.* **1996**, 57, 123–135. DOI: [https://doi.org/10.1002/\(SICI\)1097-461X\(1996\)57:1<123::AID-QUA14>3.0.CO;2-9](https://doi.org/10.1002/(SICI)1097-461X(1996)57:1<123::AID-QUA14>3.0.CO;2-9)
50. Matta, I.F., Boyd, R.J., *The Quantum Theory of Atoms in Molecules*, WILEY-VCH Verlag GmbH & Co. KGaA, Weinheim, 2007.
51. Koch, U., Popelier, P., *J. Phys. Chem. A*, **1995**, 99, 9747–9754. DOI: <https://doi.org/10.1021/j100024a016>.
52. Carroll, M. T., Bader, R. F. W., *Mol. Phys.*, **1988**, 65, 695. DOI: <http://doi.org/10.1080/00268978800101351>.
53. Cremer, D., Kraka, E., *Croat. Chem. Acta.*, **1984**, 57, 1259–1281. DOI: <https://hrcak.srce.hr/194019>
54. Rozas, I., Alkorta, I., Elguero, J., *J. Am. Chem. Soc.*, **2000**, 122, 11154–11161. DOI: <https://doi.org/10.1021/ja0017864>.
55. Bader, R. F. W., *Atoms in Molecules: A Quantum Theory* (2<sup>nd</sup> ed.) Oxford: New York, NY. 1990
56. Erdogdu, Y., Unsalan, O., Gulluoglu, M.T., *J. Raman Spectrosc.*, **2010**, 41, 820–828. DOI: <https://doi.org/10.1002/jrs.2520>
57. Erdogdu, Y., Unsalan, O., Amalanathan, M., Hubert, J. I., *J. Mol. Struct.*, **2010**, 980, 24–30. DOI: <https://doi.org/10.1016/j.molstruc.2010.06.032>
58. Gonohe, N., Abe, H., Mikami, N., Ito, M., *J. Phys. Chem.*, **1985**, 89, 3642–3648. DOI: [https://doi.org/10.1016/0009-2614\(83\)85053-2](https://doi.org/10.1016/0009-2614(83)85053-2)
59. Alyar, H., Kantarci, Z., Bahat, M., Kasap, E., *J. Mol. Struct.*, **2007**, 834, 516–520. DOI: <https://doi.org/10.1016/j.molstruc.2006.11.066>.

60. Padrón, J.A., Carasco, R., Pellón, R.F., *J. Pharm. Pharmaceut. Sci.*, **2002**, 5, 258–266.
61. Verma, R.P., Hansch, C., *Bioorg. Med. Chem.*, **2005**, 13, 2355–2372. Doi: <https://doi.org/10.1016/j.bmc.2007.01.011>.
62. Verma, R.P., Kurup, A., Hansch, C., *Bioorg. Med. Chem.*, **2005**, 13, 237–255. DOI: <https://doi.org/10.1016/j.bmc.2004.09.039>
63. Vuks, M.F., *Opt. Spectrosc.*, **1966**, 20, 361–368.
64. Kumar, A., Srivastava, A.K., Tiwari, S.N., Misra, N., Sharma, D., *Mol. Cryst. Liq. Cryst.*, **2019**, 1, 23–31.
65. Morris, G.M., Huey, R., Lindstrom, W., Sanner, M.F., Belew, R.K., Goodsell, D.S., Olson, A.J., *J. Comput. Chem.*, **2009**, 16, 2785–2791. DOI: <https://doi.org/10.1002/jcc.21256>
66. Pettersen, E.F., Goddard, T.D., Huang, C.C., Couch, G.S., Greenblatt, D.M., Meng, E.C., Ferrin, T.E., *J. Comput. Chem.* **2004**, 25, 1605–1612. DOI: <http://doi.org/10.1002/jcc.20084>
67. Morris, G.M., Goodsell, D.S., Halliday, R.S., Huey, R., Hart, W.E., Belew, R.K., Olson, A.J., *J. Comput. Chem.*, **1998**, 19, 1639–1662. DOI: [https://doi.org/10.1002/\(SICI\)1096987X\(19981115\)19:14%3C1639::AID-JCC10%3E3.0.CO;2-B](https://doi.org/10.1002/(SICI)1096987X(19981115)19:14%3C1639::AID-JCC10%3E3.0.CO;2-B).
68. *Discovery Studio 4.5 Guide*, Accelrys Inc., San Diego, 2009. <http://www.accelrys.com>
69. Oost, M., Belli, T.K., Ding, B.A., Joseph, H., Kunzer, M.K., Martineau, A., McClellan, D., Mitten, W.J., et.al, *J. Med. Chem.*, **2007**, 50, 641–662. <https://files.rcsb.org/view/2O2M.cif>.
70. Swain, S.S., Singh, S.R., Sahoo, A., Hussain, T., Pati, S., *J. Biomol. Struct. Dyn.*, **2021**, 40, 6463–6476.
71. [www.swissdock.ch](http://www.swissdock.ch)
72. Sillars-Hardebol, A. H., Carvalho, B., Beliën, J., Wit, M., Delis-van P. M. et. al., *The Journal of pathology*, **2012**, 226, 3, 442–450. DOI: <http://doi.org/10.1002/path.2983>
73. Kvensakul, M., Hinds, M.G., Banjara, S., *Biochem. J.*, **2020**, 477, 3287–3297.
74. <https://files.rcsb.org/view/6WH0.cif>.
75. <https://files.rcsb.org/view/6WGZ>.
76. Herrmann, O., Baumann, B., de Lorenzi, R., Muhammad, S., Zhang, W., Kleesiek, J., et al. *Nat. Med.*, **2005**, 12, 1322–9. DOI: <http://doi.org/10.1038/nm1323>.
77. Llona-Minguez, S., Baiget, J., Mackay, S.P., *Pharm. Pat. Anal.* **2013**, 4, 481–498. DOI: <https://doi.org/10.4155/ppa.13.31>.
78. Liu, S., Misquitta, Y.R., Olland, A., Johnson, M.A., Kelleher, K.S., Kriz, R., Lin, L.L., Stahl, M., Mosyak, L. *J Biol. Chem.*, **2013**, 288, 22758–22767. <https://www.rcsb.org/structure/4KIK>
79. Xu, G., Lo, Y.C., Li, Q., Napolitano, G., Wu, X., Jiang, X., Dreano, M., Karin, M., Wu, H., *Nature*, **2011**, 472, 325–330. <https://www.rcsb.org/structure/3rzf>